Wind and Structures, *Vol. 20, No. 6 (2015) 811-827*
DOI: http://dx.doi.org/10.12989/was.2015.20.6.811

Experimental and numerical aerodynamic investigation of a prototype vehicle

Selahaddin Orhan Akansu*[1], Yahya Erkan Akansu[2], Toygun Dagdevir[1], Ferhat Daldaban[3] and Feridun Yavas[1]

[1]*Department of Mechanical Engineering, The Faculty of Engineering of Erciyes University, Melikgazi, Kayseri 38039, Turkey*
[2]*Department of Mechanical Engineering, The Faculty of Engineering of Nigde University, Nigde 51200, Turkey*
[3]*Department of Electric & Electronic Engineering, The Faculty of Engineering Erciyes University Melikgazi, Kayseri 38039, Turkey*

(Received March 24, 2014, Revised April 10, 2015, Accepted May 3, 2015)

Abstract. This study presents experimental and numerical aerodynamic investigation of a prototype vehicle. Aerodynamics forces examined which exerted on a prototype. This experimental study was implemented in a wind tunnel for the Reynolds number between 10^5-$3.1x10^5$. Numerical aerodynamic analysis of the vehicle is conducted for different Reynolds number by using FLUENT CFD software, with the k-ε realizable turbulence model. The studied model aims at verifying the aerodynamic forces between experimental and numerical results. After the Reynolds number of $2.8x10^5$, the drag coefficient obtained experimentally becomes independent of Reynolds number and has a value of 0.25.

Keywords: vehicle aerodynamic performance; CFD (computational fluid dynamics); design codes and standards; drag coefficient; pressure distribution

1. Introduction

Automobile sector has been especially progressing since beginning of 1900s. After The Industrial Revolution, due to increasing importance of energy, studies for less fuel consumption of vehicles have increased. At first, design of automobiles were tried to be simulate with airfoils as concept designs. Recent decades, investigators have been designed new vehicles such as trains, automobiles and aircrafts by looking at the ergonomic requirements. Designs must be tested (especially experimental or numerical) to be able to employ before manufacturing. Experimenting with automobiles or even their parts can be a time consuming and expensive process. So, CFD and small scale prototype make it possible to build that can be solved to determine the pressure drop of any particular design. Cheng *et al.* (2012) investigated on numerical quantification of aerodynamic damping on pitching of vehicle-inspired bluff body. They concluded that when used in conjunction with the commonly applied drag and lift coefficients, it can improve realism in assessment of vehicle vehicle aerodynamics. Watkins and Vino (2008) investigated on the effect of vehicle spacing on

*Corresponding author, Professor, E-mail: akansu@erciyes.edu.tr

http://www.techno-press.org/?journal=was&subpage=8 ISSN: 1226-6116 (Print), 1598-6225 (Online)

the aerodynamics of a representative car shape. They stated that very significant changes in lift were also noted for close spacing and it has been revealed (via surface and off-body visualization and velocity and flow mapping) that these changes were due to the influence of the rear vortices. Due to the interest in loosely spaced vehicles (permitted via ITS) this seems to be an area where our understanding of interaction effects needs to be extended.

Conventionally, the pitching instability of road vehicles has been controlled mechanically through the application of suspension systems. Cheng *et al.* (2011) numerically investigated on transient flow past road vehicles subjected to pitching oscillation. They clarified that unsteady flow structures above the rear section of the vehicles were found to significantly affect their pitching stability; and depending on the vehicle body shape configurations, the induced aerodynamic force tended to either enhance or restrain the vehicles' pitching instability. Reynolds number, which required longer domain size downstream of the bluff body to properly reproduce the phenomena. In the case of flow past road vehicle, however, the downstream regime is dominated by a pair of longitudinal vortices and absence of the Karman vortex street. Sharma et al. (2008) investigated aerodynamics performance 1:20 scale model of a intercity bus. Also, they used CFD modelling. They stated that the magnitude and trends in the force coefficients obtained from CFD modelling exhibit remarkable agreement with experimental results. Cheli *et al.* (2011) made tests on heavy road vehicles. They measured Mean aerodynamic forces and moments by means of a six-component dynamometric balance for different yaw angles and turbulence conditions. They concluded that the vertical component is mainly affected by the detachment point of the flow in correspondence with the windward roof edge: this point, in mean turbulence condition, is moved upstream with a consequent increase of suction over the vehicle roof, finally leading to a higher upward directed vertical force. Tilch *et al.* (2008) investigated numerically on external vehicle aerodynamics. Comparisons with body-fitted and experimental data show that, this approach can yield drag predictions with an error less than 5 per cent. Simoes (2001) has studied on the design and manufacturing of a conceptual prototype vehicle. His project was the result of a collaborative project between students from the University of Aveiro and designers of the School of Arts and Design of Matosinhos. The designed vehicle (Icarus) was awarded with the first design prize and with an International Communication prize at the 1998 Shell Eco- Marathon competition. Akansu and Firat (2010) studied experimentally on square prism by slot jet injection in a wind tunnel. They stated that depending on the injection ratio, two flow regimes were obtained and a bistable mode was also observed in a transition range between them. Formula Student Racing competitions are international events like Shell Eco – Marathon have been organized among students trying to build and improve next-generation cars. Muralidharan *et al.* (2015) investigated to optimize front and rear aerodynamic wings of a high performance race car by using CFD program. They aimed to balance moment created by rear wings and concluded CL=1.89 and CD=0.909 for used economical design Selig 1223. Lu (2015) and Cheng *et al.* (2014) have investigated on drag coefficient of Formula SAE car. Cheng et al. (2014) concluded that the drag coefficient is 0.385 and the rear wings can supply 65% downforce, when the attack angle of the rear wing is set to 8°. Guilmineau (2008) investigated computationally on flow around a simplified car body. Wake flow is two-dimensional for low incidences of the rear slant, then becomes three-dimensional when the angle of the hatchback approaches 30 and reverts to two dimensional behaviour for angles higher than 301 where above this angle, a sudden drop in drag occurred. In this paper, we investigate numerically the flow around the Ahmed body for the base slant angles 251 and 351. Pinelli *et al.* (2004) measured surface pressures and overall forces of scaled models of (fire truck, ambulance, and sports utility vehicle). Han *et al.* (2013) studied on crosswind effects on high-sided road

vehicles with and without movement. They expressed that the aerodynamic force coefficients of vehicles under wind loads depend on not only the shapes of vehicles but also those of infrastructures, such as the bridge. Also they said that the aerodynamic coefficients are obviously functions of the yaw angle. Hamut *et al.* (2014) studied experimentally and numerically on effects of rear spoilers on ground vehicle aerodynamic drag. They concluded that in the CFD model, it is found that the addition of the spoiler caused a decrease in the lift coefficient from 0.26 to 0.05.

In this study, aerodynamic performance of a prototype vehicle was investigated. This study was carried out as both experimental and numerical for 100000-300000 Reynolds numbers. Also, for 251000 Reynolds Number, aerodynamic performance of a prototype vehicle was tested in different yaw angles.

2. Numerical study

CFD, Fluent package program was used as a finite volume solver for calculation of vehicle main aerodynamic characteristics. In post processing, the results which were obtained from the solution were used to compare experimental results. For the numerical calculation, two-dimensional vehicle geometry has been comprised by the side view projected area of the solid model of the prototype vehicle.

The numerical simulation was carried out by using the Navier-Stokes equation based on the 2D. The density and dynamic viscosity were constant and the flow was steady. Numerical computations were carried out by the finite volume method with unstructured grid method. The general form of the continuity Eq. (1) and the momentum Eq. (2) were shown as below

$$\frac{\partial \rho}{\partial t} + \frac{\partial (\rho u_j)}{\partial x_j} = 0 \tag{1}$$

$$\frac{\partial (\rho u_i)}{\partial t} + \frac{\partial (\rho u_i u_j)}{\partial x_j} = \frac{\partial \left[\mu_e \left(\frac{\partial u_i}{\partial x_j} + \frac{\partial u_j}{\partial x_i}\right)\right]}{\partial x_j} - \frac{\partial P}{\partial x_j} + S_i \tag{2}$$

Where ρ is fluid density (kg/m^3), the x_j is coordinate component, $u_i u_j$ is the average relative velocity components, ω_k is the significant viscosity coefficient, P is the pressure (Pa), S_i is the generated item.

The modelled transport equations for k and ε in the realizable k - ϵ model are

$$\frac{\partial}{\partial t}(\rho k) + \frac{\partial}{\partial u_j}(\rho k u_j) = \frac{\partial}{\partial x_j}\left[\left(\mu + \frac{\mu_t}{\sigma_k}\right)\frac{\partial k}{\partial x_j}\right] + G_k + G_b - \rho\epsilon - Y_M + S_k \tag{3}$$

$$\frac{\partial (\rho\epsilon)}{\partial t} + \frac{\partial (\rho\epsilon u_j)}{\partial x_j} = \frac{\partial}{\partial x_j}\left[\left(\mu + \frac{\mu_t}{\sigma_\epsilon}\right)\frac{\partial \epsilon}{\partial x_j}\right] + \rho C_1 S_\epsilon - \rho C_2 \frac{\epsilon^2}{k + \sqrt{\nu\epsilon}} + C_{1\epsilon}\frac{\epsilon}{k} C_{3\epsilon} G_b + S_\epsilon \tag{4}$$

Where

$$C_1 = \max[0.43 \frac{\eta}{\eta+5}] \quad , \qquad \eta = S\frac{k}{\epsilon} \ , \qquad S = \sqrt{2 S_{ij} S_{ij}}$$

In these equations, Gk represents the generation of turbulence kinetic energy due to the mean velocity gradients, calculated in same manner as standard k-epsilon model Gb is the generation of turbulence kinetic energy due to buoyancy, calculated in same way as standard k-epsilon model.

2.1 Modelling turbulent viscosity

$$\mu_t = \rho C_\mu \frac{k^2}{\epsilon} \tag{5}$$

Where

$$C_\mu = \frac{1}{A_0 + A_s \frac{kU^*}{\epsilon}}$$
$$U^* \equiv \sqrt{S_{ij}S_{ij} + \acute{\Omega}_{ij}\acute{\Omega}_{ij}} \;;$$
$$\acute{\Omega}_{ij} = \Omega_{ij} - 2\epsilon_{ijk}\omega_k$$
$$\Omega_{ij} = \widetilde{\Omega} - \epsilon_{ijk}\omega_k$$

Where $\widetilde{\Omega}$ is the mean rate of rotation tensor viewed in a rotating reference frame with the angular velocity ω_k. The model constants A_0 and A_s are given by (Fluent Inc 2006)

$$A_0 = 4.04,\ A_s = \sqrt{6}\cos\phi$$
$$\Phi = \frac{1}{3}cos^{-1}\left(\sqrt{6}W\right),\ W = \frac{S_{ij}S_{jk}S_{ki}}{\check{S}^3},\quad \check{S} = \sqrt{S_{ij}S_{ij}},\quad S_{ij} = \frac{1}{2}\left(\frac{\partial U_j}{\partial x_i} + \frac{\partial U_i}{\partial x_j}\right)$$

2.2. Model constants

$C_{1\epsilon} = 1.44$, $C_2 = 1.9$, $\sigma_k = 1.0$, $\sigma_\epsilon = 1.2$
σ_k : TKE Prandtl Number
σ_ϵ : TDR Prandtl Number

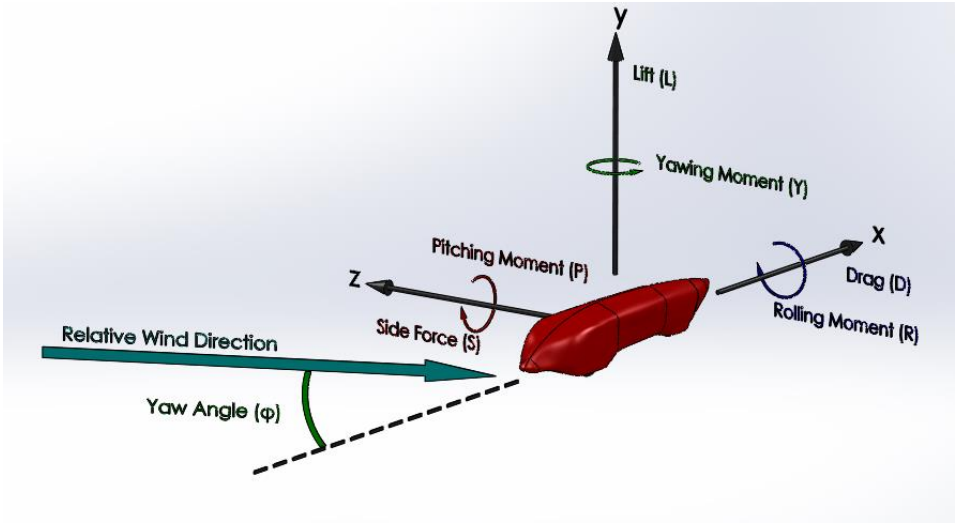

Fig. 1 Forces and moments which effect on the vehicle

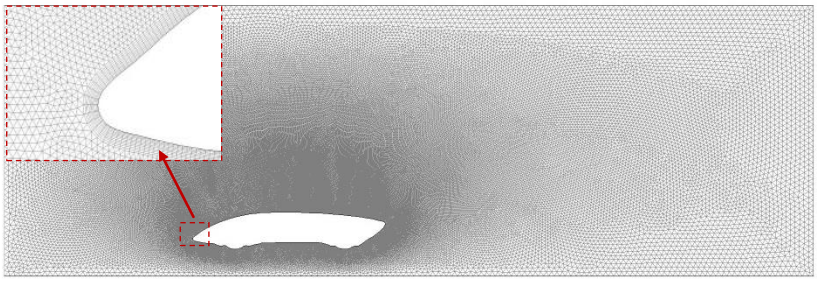

Fig. 2 The mesh structure around the vehicle

Drag force which helps to explain vehicle aerodynamic characteristic were obtained in CFD and its dimensionless form of drag coefficient were calculated for the reference values. Fig. 1 shows the forces and moments acting on a vehicle as drag force (F_D), lift force (F_L), yawing force (F_Y), pitching moment (M_P), rolling moment (M_R), yawing moment (M_Y). In this study, it is focused on the drag force acting on the vehicle. Fig. 2 shows mesh structure around the model. Structured boundary mesh around the model and unstructured triangle mesh in the rest of the flow field have been used. The mesh number has been defined after the grid independence test. The test has been implemented for the mesh numbers of 50450, 151200, 169500, 183400 and 248000. 169500 meshes have been used in this study which has sufficient to being verifying results of solutions are steady.

3. Experimental study

The experiments were conducted in 100000-314000 Reynolds numbers, suction-type wind tunnel with a square test section of 405 mm × 405 mm. The cross section area ratio of the tunnel contraction cone was 9:1 and the side walls of the test section were expanded with a divergence angle of 0.3° on each side to give a constant static pressure and to compensate for the boundary layer growth along the test section. The blockage ratio of the model was less than %2 in the test section.

The schematic diagram of the experimental setup is shown in Fig. 3. The 1/8 scaled test model vehicle the test section and was centred on the mid-height of the test section. Length of the test model is 358 mm. Firstly, the force measurements at different Reynolds numbers and at yaw angles were carried out. In the force measurement, ATI Gamma model 6-component loadcell were used. The yaw angle was controlled by computer aided rotary unit which connected to loadcell. The measurements were conducted in 500Hz sampling frequency and 10000 samples were collected by the data acquisition system during 20s. Also, each measurement repeated 3 times to eliminate the measurement errors. Then, the force data are reduced to drag and lift coefficient by using the Eqs. (7) and (8).

Pressure measurements were performed case of zero attack angles. In the wind tunnel test region, the test model was located 40 mm higher than bottom and on 300 mm x 380 mm plate. Force and pressure measurement was carried out in 100000-314000 Reynolds numbers. Ambient pressure and temperature values were 86 kPa and 26.3°C, respectively. For pressure measurements, PX-278-01D5V model pressure transducer was used. For each pressure measurement, numbers of

4048 data were read. The numbers of pressure tap were 39 (23 numbers of pressure taps was upper and 16 number was bottom). Sampling rate is 200 Hz and each measurement time was 20.24 second.

Fig. 4 shows cross section of test model and the measurement system. The pressure coefficient (C_p) is a dimensionless number which describes the relative pressures throughout a flow field in fluid dynamics.

$$C_p = \frac{P - P_\infty}{1/2 \rho U_\infty^2} \tag{6}$$

Where, P is the surface pressure at the any point of model, P∞ is the static pressure in the free stream region, ρ is the free stream fluid density , U_∞ is the free stream velocity of the fluid.

The drag coefficient Cd and lift coefficient C_L are defined as

$$C_D = \frac{F_D}{1/2 \rho U_{\infty A}^2} \tag{7}$$

$$C_L = \frac{F_L}{1/2 \rho U_\infty^2 A_s} \tag{8}$$

Where, F_D and F_L are lift and drag force, respectively. A and A_s are reference and span area of model.

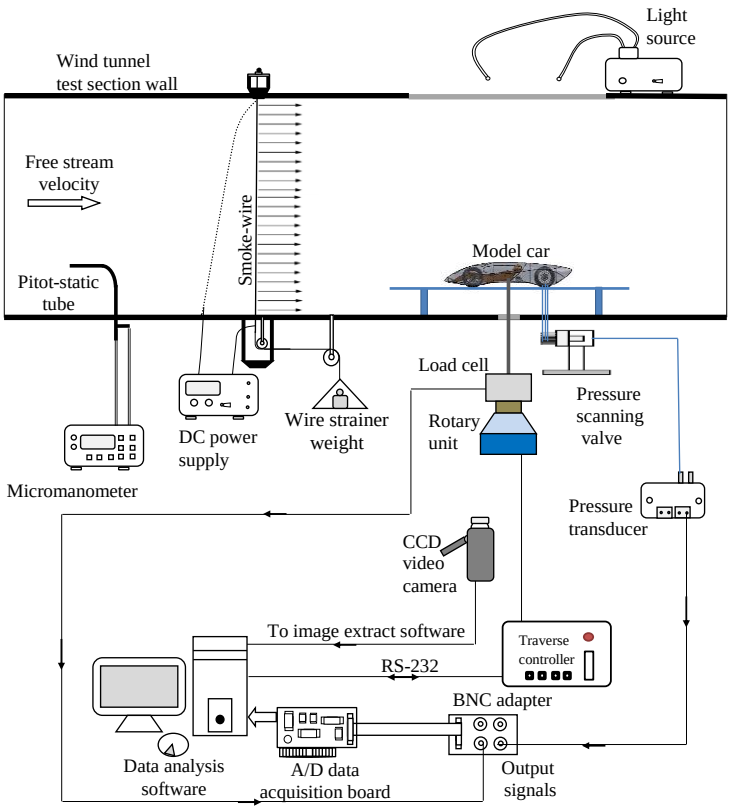

Fig. 3 The schematic diagram of the experimental setup

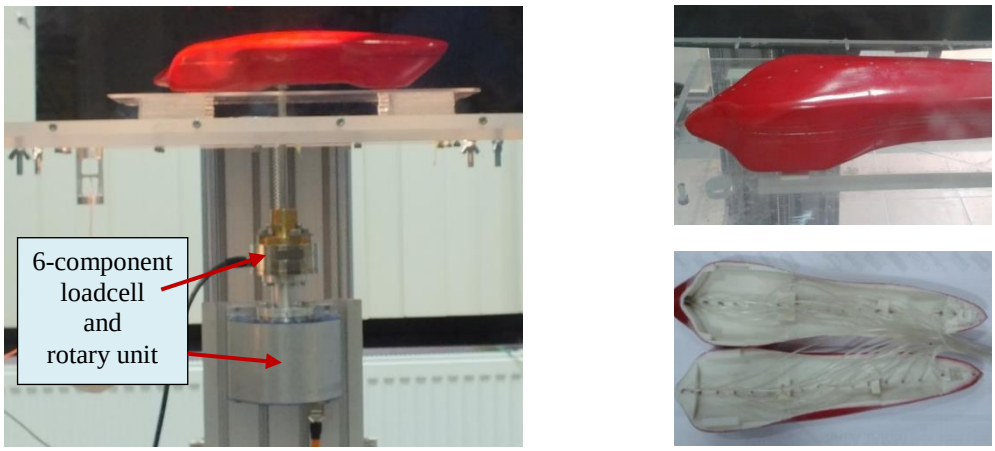

Fig. 4 Measurements of force and pressure taps at upper and bottom surface of prototype

4. Results and discussion

The average drag coefficients of cars dropped to around 0.30 for today's vehicles. This coefficient can be more reduced, but this is achieved after making the comfort of drivers a seconder consideration. Tried to improve features of current cars to utilize in future, by improving design of prototype vehicles. So, this is a transition period from concept cars to cars on road. In this scope, a lot of investigations were conducted numerically and experimentally to reduce the drag coefficient and drag coefficient of sportive urban cars is generally around 0.35, as Hassan *et al*. (2014), Khaled *et al*. (2012) numerically and Zhang *et al*. (2014) experimentally examined. There is another study investigated by Nasir *et al*. (2012) which is aerodynamics of ARTeC's PEC 2011 EMo-C Car. They found that the drag coefficient of prototype vehicle of 0.42 and 0.48; numerically and experimentally, respectively. Also almost all famous car companies calculated and informed (URL-1) average drag coefficient values of their car models that are of around 0.30. However, drag coefficient of Toyota Prius which has the lowest drag coefficient is 0.26 (Cengel 2006).

The numerical method is validated by using the comparison between the numerical and experimental drag coefficient for 10^5-$3.1x10^5$ Reynolds numbers. Fig. 5 shows C_D drag coefficients versus the Reynolds number. After the Reynolds number of $2.8x10^5$, the drag coefficient obtained experimentally becomes independent of Reynolds number and has a value of 0.25. Although the numerical calculations obtained for 2D vehicle geometry, the numerical and experimental results are supportive of each other.

From the Fig. 5, it can be seen that at low Reynolds number, the drag coefficient increases and then decreases as a result of the change in the flow structure due to the transition from laminar to turbulence boundary layer on the test model. This case is associated with the pressure distributions given in Figs. 6 and 7. The pressure level on the front and back surface of the prototype changes with the increasing Reynolds number. When looking at the pressure values taken on the vicinity of stagnation point of the model, the maximum pressure was occurred at the Reynolds number of $1.5x10^5$. The pressure on the back side surface of the model proportionally increases with the

increasing Reynolds number affecting the drag coefficient to be reduced. The pressure distribution on the front and back side surfaces of the model is related with the pressure based drag force.

Figs. 6 and 7 depict pressure coefficient for upper and bottom surface versus vehicle length (x/L), respectively.

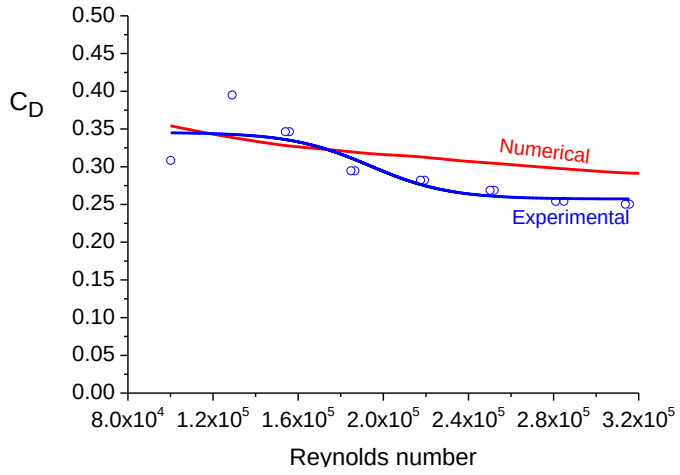

Fig. 5 Drag coefficients versus Reynolds number

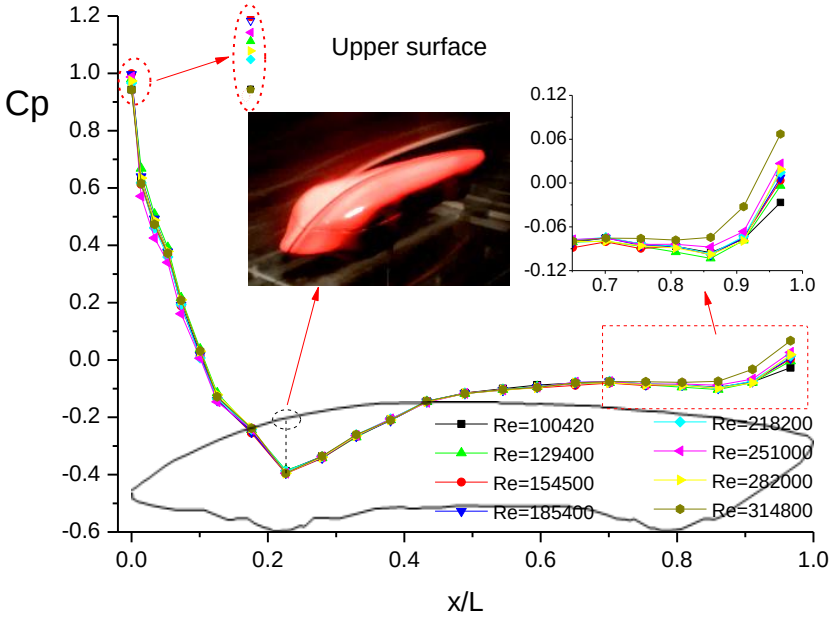

Fig. 6 The pressure coefficient for upper surface versus vehicle length (x/L)

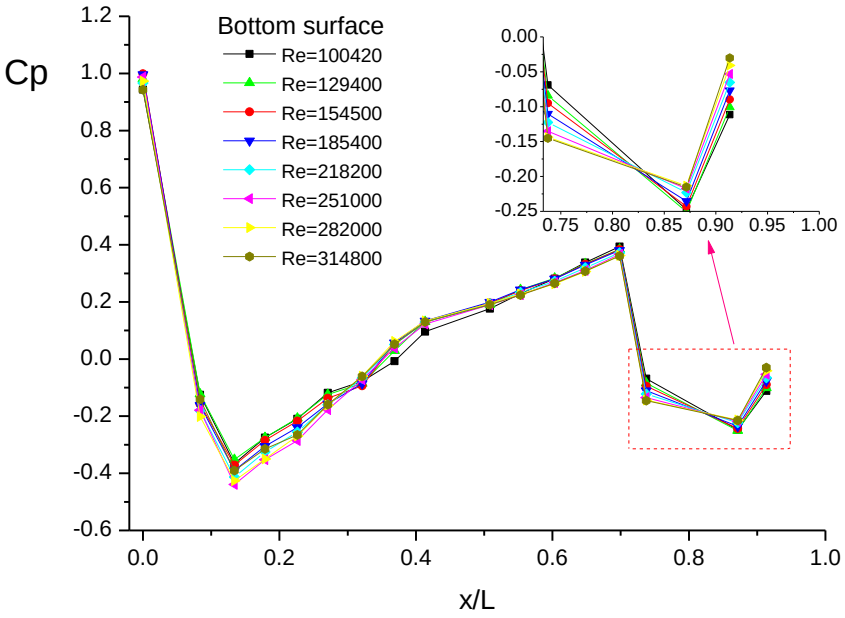

Fig. 7 The pressure coefficient for bottom surface versus vehicle length (x/L)

As seen Figs. 6 and 7, the pressure coefficients values have a little difference in values depending on the Reynolds number. The pressure distribution on the upper surface has similar characteristics with an airfoil. The highest pressure coefficient values have been obtained at the tip of vehicle. The value of the Cp is near 1 due to stagnation point. In the upper surface, pressure coefficient values decrease until x/L =0.22; depend on the increase in the velocity over front surface. Due to the boundary layer development and flow separation, the velocity decreases and the value of pressure coefficient tends to increase up to x/L=0.5. The flow separation can be seen on the symmetry plane by the smoke-wire flow visualization (Fig. 6). After the maximum height location, the separated shear layer continues to flow near the surface and the level of the pressure coefficient has a value in the vicinity of 0 up to x/L=0.9. As a result of the afterbody shape, there is an additional pressure recovery on the trailing edge of the model.

On the bottom surface of the vehicle, the pressure coefficient changes according to the geometry of model and the distance between the ground and the bottom surface of the vehicle. After the stagnation point, pressure coefficient values reduce quickly up to x/L=0.13 and then depend on the bottom shape of vehicle, which is concave surface between the front wheels, volume is expand between the ground and the vehicle, so velocity values decrease by causing increase in the pressure coefficients. The rear wheel is on the symmetry axis of the vehicle and it obstructs the flow. This is the reason of the positive pressure coefficient before the rear wheel.

To show the comparison between the numerical and experimental results, the pressure distributions around the vehicle at the mid-span center plane were given Fig. 8. In contrast to upper surface pressure distribution, the numerical and experimental results on the bottom surface are closer (more near) to each other. For the upper surface, after the stagnation point, the pressure distribution obtained from the experiments has higher values than the numerical one. This

difference would be expected for the 2D numerical solution. It is well known that the pressure distribution is effected from the three dimensional flow field around a circular cylinder which has a small aspect ratio without end plate (Bearman ve Wadcock 1973). Therefore, discrepancies between the experimental and numeric results are due to fact that the 2D numerical model doesn't include 3D effects of the real vehicle geometry.

Fig. 9 illustrates that the stream lines around the vehicle for the Reynolds number of $3.14x10^5$. The test model has slightly curved shape at the upper surface and afterbofy shape like a beak at the rear of the vehicle. The free stream divides into two patterns and above and below stream lines show a narrower wake region behind the vehicle which corresponds a reduction in the drag.

Fig. 10 displays the static pressure around the vehicle for Re=3.14x105. As expected, maximum pressure occurs at tip of the vehicle and being low pressure at the upper surface of vehicle. By means of the afterbody shape of the vehicle, the pressure recovery on the rear side causes to decrease in the pressure based drag forces. As can be seen in Fig. 11, velocity contour is granted to illustrate fast, low and zero flow velocities. It is obvious that the decreased velocity field occurs in the wake of the vehicle.

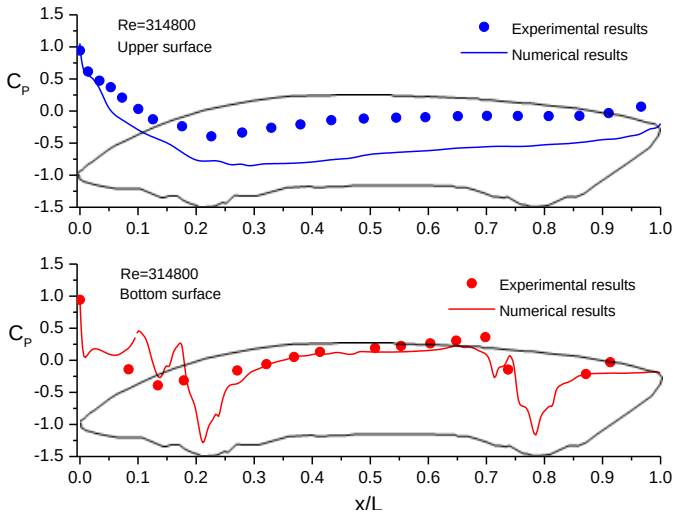

Fig. 8 The pressure coefficient distributions for the Reynolds number of $3.14x10^5$

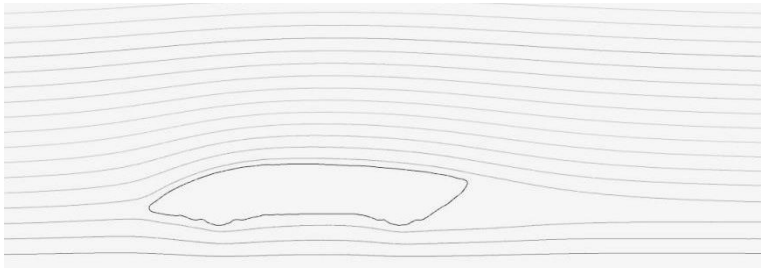

Fig. 9 The stream lines around the vehicle for the Reynolds number of $3.14x10^5$

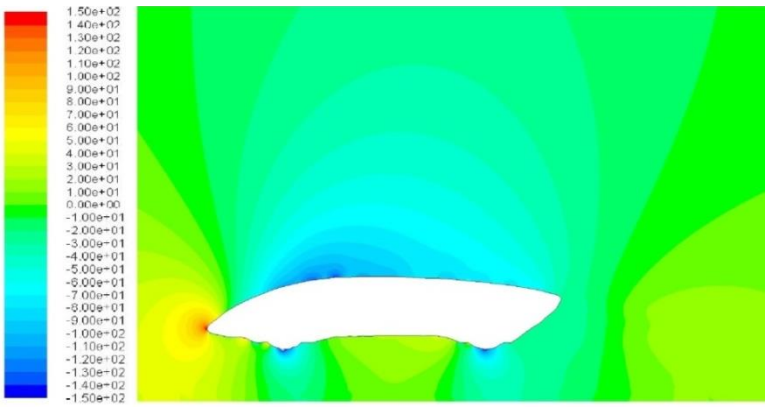

Fig. 10 The static pressure [Pa] contours around the vehicle for the Reynolds number of $3.14x10^5$

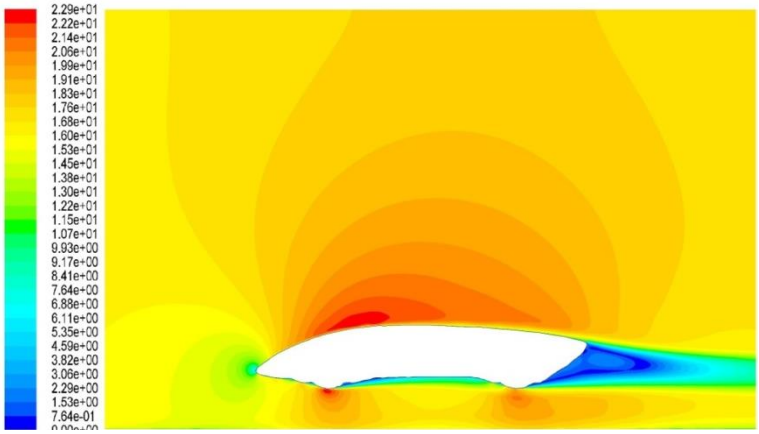

Fig. 11 The velocity magnitude [m/s] contours around the vehicle for the Reynolds number of $3.14x10^5$

Fig. 12 shows velocity contours at Reynolds number of (a) 314800, (b) 251000, (c) 185400 and (d) 100400 in numerical study. Velocity values near the vehicle's upper region are the highest. The air velocity increases on the vehicle upper surface and it provides that pressure decreases. The recirculation region occurs near the vehicle's bottom wheels and vehicle's back area in all cases.

C_L is the coefficient of aerodynamic lift obtained from the wind tunnel testing. Typical values of C_L for passenger cars vary in the range of 0.2-0.5 using the frontal area of vehicle as the characteristic area. Similar to coefficient of aerodynamic resistance, it depends not only on the shape of vehicle, but also on a number of operation factor (Wong 2008). Fig. 13 shows C_L values versus the Reynolds Numbers. C_L values fully depend on the Reynolds number and they are measured between -0.03 and 0.1. It may be considered that these values are very low levels and change excursively with Reynolds number for this vehicle. Especially, the negative lift force acts as a downforce to the vehicle. The downforce increases load on the tires and improve cornering performance.

The yaw angle is the angle between a line pointing in the direction the car is moving and the car's x-axis (which is the direction the car is pointed). In the simplest case (shown on the left side of the drawing), the car is travelling straight and is pointed in exactly the same direction it is travelling, so it has no yaw. The car on the right is yawed, which means that the car is headed in a different direction than it is pointing (Fig. 14) (URL-2).

Fig. 15 and 16 show the drag and lift coefficients respectively in different yaw angle for Reynolds Number of $2.5x10^5$. The drag coefficient and lift coefficient increase with increasing the yaw angle. Although the drag coefficient is small at zero yaw angle, significant side force causes to increase in the drag and lift coefficients by the increase of the angle.

After these aerodynamic tests, Mobydick (name of the vehicle) was begun to produce. Manufacturing of the chassis, cockpit, transmission driven train, braking system and steering system, engine modifications and adaptations, electronics and telemetry implementation of vehicle were occurred. The Mobydick was joined the Shell-Eco Marathon race. Fig. 16 shows photo of Mobydick at Shell Eco Marathon competition (2011).

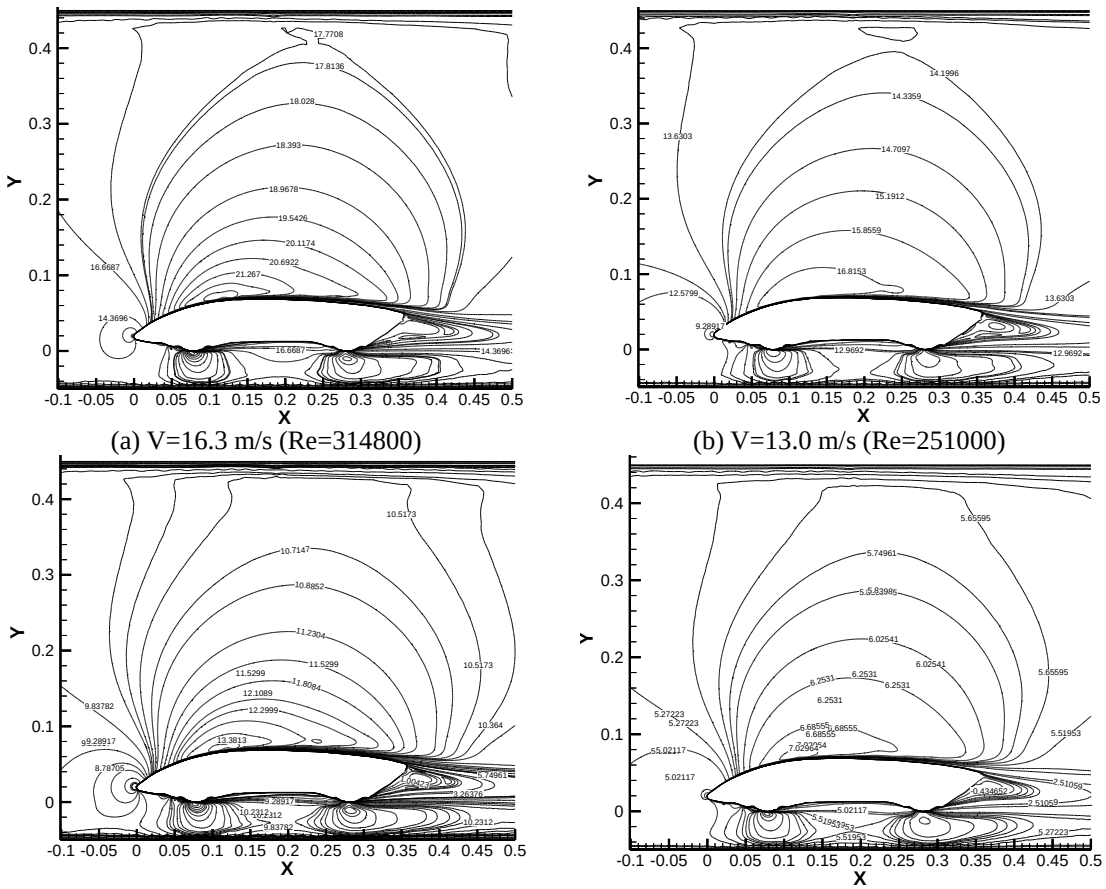

(a) V=16.3 m/s (Re=314800)

(b) V=13.0 m/s (Re=251000)

(c) V=9.7 m/s (Re=185400)

(d) V=5.2 m/s (Re=100400)

Fig. 12 Velocity contours on different velocities

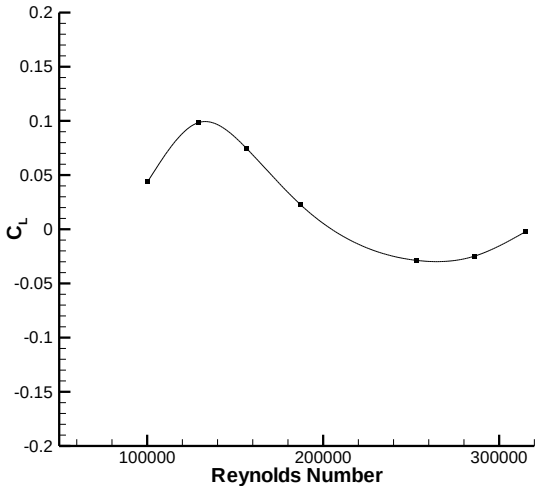

Fig. 13 C_L values versus the Reynolds Numbers

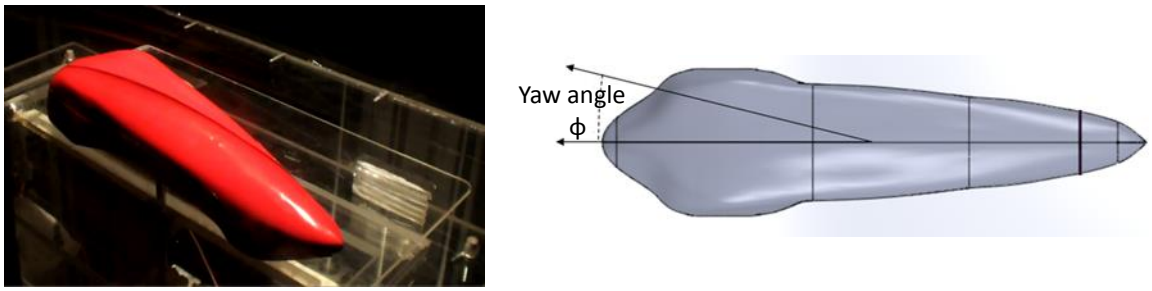

Fig. 14 Tested prototype vehicle in different yaw angle

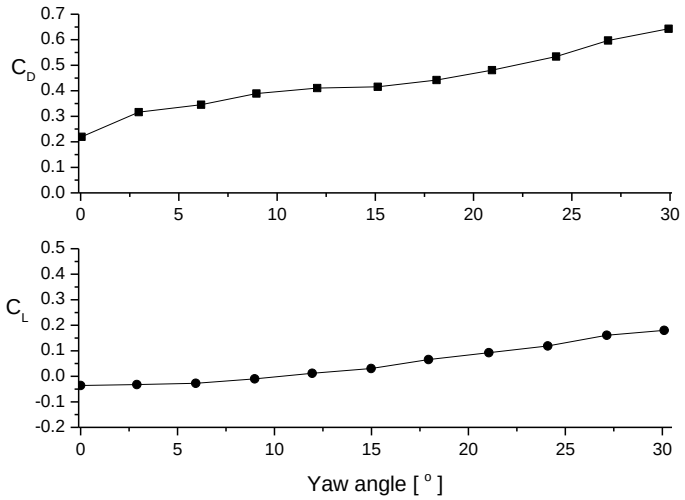

Fig. 15 Drag and lift coefficient values of prototype versus the yaw angle at 251000 Reynolds Number

Fig. 16 Mobydick at Shell Eco Marathon competition (2011)

5. Conclusions

Mobydick was designed by Erciyes University students, which the prototype was produced in scaled 1/8. Aerodynamic tests of the prototype were implemented at Nigde University. Manufacturing of mobydick was carried out at Erciyes University. Numerical and experimental analysis of aerodynamic for Mobydick prototype is examined in zero yaw angle for $1.0x10^5$-$3.1x10^5$ Reynolds number and in 0°-30° yaw angles for $2.5x10^5$ Reynolds numbers.

- The drag coefficient has a value of 0.25 after the Reynolds number of $2.8x10^5$.
- The drag coefficient value reduces depends on increasing Reynolds Number.
- Numerical and experimental analysis showed mostly compliance among each other. Discrepancies between experimental and numeric study are due to fact that 2D properties do not wholly include 3D properties.
- The obtained lift coefficient is lower than 0.1.
- The highest pressure coefficient value was obtained on the tip of the vehicle at the stagnation point. In the upper surface, the minimum pressure coefficient value was determined at the flow separation point.
- As the yaw angle increases, the drag and lift coefficient value increases due to the long shape of the vehicle.

Consequently, in respect of the vehicle aerodynamics, the sciences of materials, structural mechanics, CAD-CAM are involved in the production of a conceptual vehicle.

Acknowledgements

The authors would like to thank all students, designers and teachers involved in the Mobydick project. The authors would also like to thank to the Erciyes University research fund (project no: FBA-11-3453).

References

Akansu, Y.E. and Firat, E. (2010), "Control of flow around a square prism by slot jet injection from the rear surface", *Expert. Therm. Fluid Sci*., **34**(7), 906-914.

Bearman, P.W. and Wadcock, A.J. (1973), "The interaction between a pair of circular cylinders normal to a stream", *J. Fluid Mech*., **61**, 499-511

Cengel, Y.A. and Cimbala, J.M. (2006), *Fluid Mechanics Fundamentals and Application McGraw-Hill Companies*, New York, USA.

Cheli, F., Corradi, R., Sabbioni, E. and Tomasini, G. (2011), "Wind tunnel tests on heavy road vehicles : Cross wind induced loads-Part 1", *J. Wind Eng. Ind. Aerod*., **99**(10), 1000-1010.

Cheng, S.Y., Tsubokura, M., Nakashima, T., Nouzawa, T. and Okada, Y. (2011), "A numerical analysis of transient flow past road vehicles subjected to pitching oscillation", *J. Wind Eng. Ind. Aerod*., **99**(5), 511-522.

Cheng, S.Y., Tsubokura, M., Nakashima, T., Okada, Y. and Nouzawa, T. (2012), "Numerical quantification of aerodynamic damping on pitching of vehicle-inspired bluff body", *J. Fluids Struct.*, **30**, 188-204.

Cheng, X.H., Luo, S.M., Chang, X.F. and Xie, D. (2014), "Numerical analysis of an external Flow-Field around a Formula SAE Car Body Based on FLUENT", *Adv. Mater. Res.*, **1039**, 17-24.

Fluent Inc. (2006), *Fluent 6.3 User's Guide*, Lebanon, New Hampshire.

Guilmineau, E. (2008), "Computational study of flow around a simplified car body", *J. Wind Eng. Ind. Aerod.*, **96**(6-7), 1207-1217

Hamut, S.H., El-Emam, R.S., Aydin, M. and Dincer, I. (2014), "Effects of rear poilers on ground vehicle aerodynamic drag", *Int. J. Numer.Method. Heat Fluid*, **24**(3), 627-642.

Han, Y., Hui, J., Cai, C.S., Chen, Z. and Li, C. (2013), " Experimental and numerical studies of aerodynamic forces on vehicles and bridges", *Wind Struct*., **17**(2), 163-184.

Hassan, S.M.R., Islam, T., Ali, M. and Islam, M.Q. (2014), "Numerical study on aerodynamic drag reduction of racing cars", *Procedia Eng*., **90**, 308-313.

Khaled, M., Hage, H.E., Harambat, F. and Peerhossaini, H. (2012), "Some innovative concepts for car drag reduction: A parametric analysis of aerodynamic forces on a simplified body", *J. Wind Eng. Ind. Aerod.*, **107-108**, 36-47.

Lu, X. (2015), *Research on the Flow Field around a Formula SAE Car*, SAE Technical Paper. no: 2015-26-0208.

Muralidharan, V., Balakrishnan, A. and Kumar, Y.S. (2015), "Desing optimization of front and rear aerodynamic wings of a high performance race car with modified airfoil structure", *Nascent Technologies in the Engineering Field (ICNTE*), Mumbai, Jan.

Nasir, R.E.M., Mohamad, F., Kasiran, R. and Adenan, M.S., Mohamed, M.F., Mat, M.H. and Ghani, A.R.A. (2012), "Aerodynamics of ARTeC's PEC 2011 EMo-C Car", *Procedia Eng*., **41**, 1775-1780.

Pinelli, J.P., Subramanian, C. and Plamondon M. (2004), "Wind effects on emergency vehicles", *J. Wind Eng. Ind. Aerod.*, **92**(7-8), 663-685.

Sharma, R., Chadwick, D. and Haines, J. (2008), "Aerodynamics of an intercity bus", *Wind Struct*., **11**(4), 257-273.

Simoes J.A.O. (2001), "Icarus: the design process of a conceptual vehicle", *Mater. Des.*, **22**(4), 251-257.

Tilch, R., Tabbal, A., Zhu, M., Decker, F. and Löhner, R. (2008), "Combination of body-fitted and embedded grids for external vehicle aerodynamics", *Eng. Comput*., **25**(1), 28-41

Watkins, S. and Vino, G. (2008), "The effect of vehicle spacing on the aerodynamics of a representative car shape", *J. Wind Eng. Ind. Aerod*., **96**(6-7), 1232-1239.

Wong, J.Y. (2008), *Theory of Ground Vehicles*, John Wiley& Sons, Hoboken, New Jersey, USA.

Zhang, Y.C., Ding, W., Zhang, Z. and Li, J. (2014), "Comparison research on aerodynamic drags and pressure coefficients of reference car models in automotive wind tunnel", *Adv. Mater. Res*., **989-994**, 2834-2838.

Website links

URL-1: http://en.wikipedia.org/wiki/Automobile_drag_coefficient, April 2015
URL-2: http://www.formula1-dictionary.net/yaw.html.

CC

Nomenclature

A [m^2]	reference area of model
As [m^2]	span area of model
C_P [-]	pressure coefficient
C_L [-]	lift coefficient
C_D [-]	drag coefficient
F_D [N]	drag force
F_L [N]	lift force
F_Y [N]	yawing force
M_P [Nm]	pitching moment
M_R [Nm]	rolling moment
M_Y [Nm]	yawing moment
P_∞ [Pa]	static pressure in the free stream region
u [m/s]	average relative velocity
k [m^2/s^3]	turbulent kinetic energy
ϵ [-]	turbulent energy dissipation rate
Φ [°]	yaw angle
P [Pa]	pressure
Re	Reynolds number
Re_{cr}	critical Reynolds number
U_∞ [m/s]	free stream velocity of the fluid
μ [Pa·s]	dynamic viscosity
ρ [kg/m^3]	air density
σ_k [-]	TKE Prandtl Number
σ_ϵ [-]	TDR Prandtl Number